Structural Engineering and Mechanics, Vol. 11, No. 5 (2001) 547-564
DOI: http://dx.doi.org/10.12989/sem.2001.11.5.547

A two-phase interface element for simulation of lining systems

X. Liu†, A. Scarpas‡ and J. Blaauwendraad‡†

Department of Civil Engineering and Geosciences, Delft University of Technology, Stevinweg 1, 2628CN Delft, The Netherlands

Abstract. The numerical formulation of a two-phase interface element appropriate for porous lining system is presented. The formulation is isoparametric and can be applied both for 2-D and 3-D analysis. Biot's theory is utilized as the basis for the development of the element constitutive theory. In order to be capable of simulating the reinforcing characteristics of some geotextiles utilized as lining system, a reinforcement component has also been implemented into the formulation. By employing this specially developed interface finite element, the influence of soil consolidation on the stress distribution along the lining system of a reservoir and a landfill has been investigated.

Key words: Interface element; porous media; two-phase; lining system; finite element; consolidation; reinforcement; reservoir; landfill.

1. Introduction

Lining systems (LS) are widely utilized in several areas of environmental, transportation and geotechnical engineering. For instance, low permeability LS (geomembranes) act as barriers in landfills or reservoir structures to control fluid migration Fig. 1. High tension stiffness LS (geotextiles or geogrids) perform draining, separating or reinforcing functions in road and other constructions.

The thickness of a LS is typically very small in comparison to the lateral dimensions. In the context of the finite element method, the artifice of degenerating ordinary continuous finite elements into elements of very small thickness renders the elements grossly inaccurate. As a result, for adequate modeling of this type of LS, a special type of finite elements interface elements has been formulated.

Interface elements have been widely used in the past for the simulation of geometrical discontinuities within structures (Plesha *et al.* 1989, Mehlhorn *et al.* 1985, Gens *et al*. 1988, Schellekens 1990, Scarpas *et al*. 1994).

In the case of flow through porous LS, in addition to the solid phase, the fluid phase must also be taken into account. In this contribution, a two-phase interface finite element has been formulated capable of simulating the interaction between the mechanical behavior of the solid phase and the flow characteristics of the liquid phase (Fig. 1).

† Researcher
‡ Associate Professor
‡† Professor

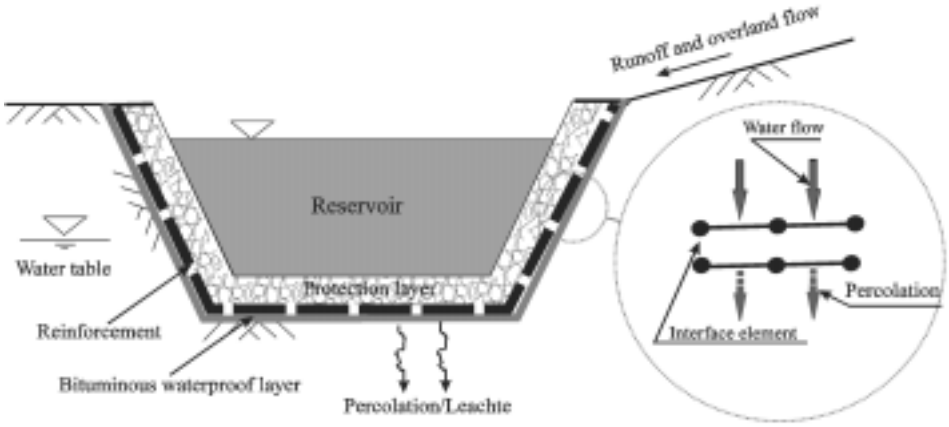

Fig. 1 Schematic of bituminous waterproof LS in reservoir (Liu *et al*. 1999)

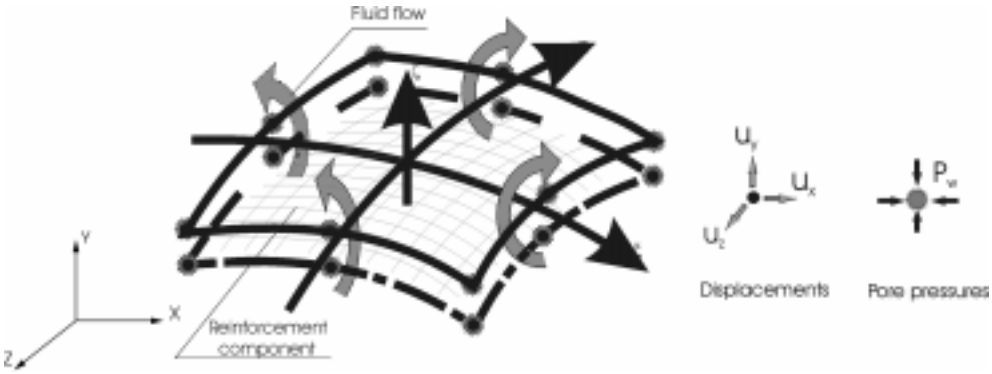

Fig. 2 Schematic of an interface element for two-phase media (Liu *et al.* 1999)

Biot's theory is the basis for the development of the governing equations. In its 3D configuration, the element consists of 16 nodes (Fig. 2). To each node correspond three displacement degrees of freedom and a fourth one associated with the pore pressure of the liquid phase. An orthotropic formulation of the permeability characteristics of the element enables simulation of directional flow patterns within the element.

In order to be capable of simulating reinforcing characteristics of geotextiles utilized as LS, a reinforcement component has also been implemented into this element (Fig. 2).

Implementation of the element into the finite element system INSAP-PM, developed at TU-Delft, enabled the investigation of the development and distribution of forces in LS and their variation in time. In the following various aspects of the element formulation are discussed.

2. Nodal components interpolation

2.1 Solid component

The two-phase interface element shown in Fig. 2, consists of two overlapping planes, each defined

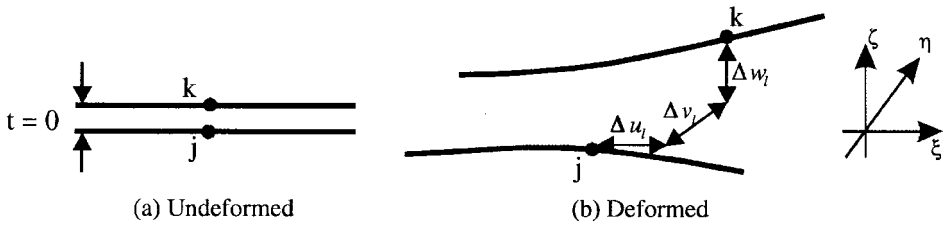

Fig. 3 Interface element relative displacements

by a set of 8 nodes. The thickness of the element in its undeformed configuration can be specified to be zero.

According to the standard isoparametric formulation, the global coordinates can be expressed in terms of the coordinates of the element nodes by the mapping:

$$x=\sum_{i=1}^{8} \boldsymbol{N}_i \cdot x_i,\ \ y=\sum_{i=1}^{8} \boldsymbol{N}_i \cdot y_i,\ \ z=\sum_{i=1}^{8} \boldsymbol{N}_i \cdot z_i \tag{1}$$

in which $\boldsymbol{N}_i$ are the standard isoparametric shape functions. It is worth noticing that in contrast to the classical theory, the summation of Eq. (1), which defines the coordinate interpolation, spans only over the nodes on one side of the element mid-plane and not over the total number of nodes.

In the local coordinate system, the relative displacements between two originally coinciding points *j* and *k*, one on each side of the element, Fig. 3, can be computed from:

$$\begin{Bmatrix} \Delta u_l \\ \Delta v_l \\ \Delta w_l \end{Bmatrix} = \begin{bmatrix} 1 & 0 & 0 & -1 & 0 & 0 \\ 0 & 1 & 0 & 0 & -1 & 0 \\ 0 & 0 & 1 & 0 & 0 & -1 \end{bmatrix} \cdot \begin{Bmatrix} u_l^k \\ v_l^k \\ w_l^k \\ u_l^j \\ v_l^j \\ w_l^j \end{Bmatrix} \tag{2a}$$

or

$$_{if}\boldsymbol{\varepsilon}_l = \boldsymbol{L} \cdot \boldsymbol{u}_l \tag{2b}$$

in which the subscript *l* denotes displacements in the local axes system and the notation $_{if}\boldsymbol{\varepsilon}_l$ has been adopted for the relative displacements to denote the fact that they play the role of "equivalent strain" in all subsequent derivations.

Utilizing the same isoparametric interpolation as for the coordinates, the global displacements between the above two points, Fig. 3, can be expressed in terms of the nodal displacements as:

$$\begin{Bmatrix} u^k \\ v^k \\ w^k \\ u^j \\ v^j \\ w^j \end{Bmatrix} = \begin{bmatrix} 0 & 0 & 0 & 0 & \cdots & 0 & 0 & 0 & N_1 & 0 & 0 & N_2 & \cdots & N_8 & 0 & 0 \\ 0 & 0 & 0 & 0 & \cdots & 0 & 0 & 0 & 0 & N_1 & 0 & 0 & \cdots & 0 & N_8 & 0 \\ 0 & 0 & 0 & 0 & \cdots & 0 & 0 & 0 & 0 & 0 & N_1 & 0 & \cdots & 0 & 0 & N_8 \\ N_1 & 0 & 0 & N_2 & \cdots & N_8 & 0 & 0 & 0 & 0 & 0 & 0 & \cdots & 0 & 0 & 0 \\ 0 & N_1 & 0 & 0 & \cdots & 0 & N_8 & 0 & 0 & 0 & 0 & 0 & \cdots & 0 & 0 & 0 \\ 0 & 0 & N_1 & 0 & \cdots & 0 & 0 & N_8 & 0 & 0 & 0 & 0 & \cdots & 0 & 0 & 0 \end{bmatrix} \cdot \begin{bmatrix} u_1 \\ v_1 \\ w_1 \\ u_2 \\ v_2 \\ \cdots \\ \cdots \\ v_{15} \\ w_{15} \\ u_{16} \\ v_{16} \\ w_{16} \end{bmatrix} \tag{3a}$$

or

$$\boldsymbol{u} = \boldsymbol{N} \cdot \bar{\boldsymbol{u}} \tag{3b}$$

If the element local axes are inclined at an angle θ with respect to the global axes then, the relation between local interface displacements $\boldsymbol{u}_l$ and the corresponding global displacements $\boldsymbol{u}$ is:

$$\boldsymbol{u}_l = \boldsymbol{T} \cdot \boldsymbol{u} \tag{4}$$

in which $\boldsymbol{T}$ is the standard transformation matrix from the global to the local coordinate system.

Successively substituting Eq. (2) into Eq. (4) and the latter into Eq. (3b), the equivalent strains ${}_{if}\boldsymbol{\varepsilon}_l$ in the local element axes system can be expressed as:

$${}_{if}\boldsymbol{\varepsilon}_l = \boldsymbol{L} \cdot \boldsymbol{T} \cdot \bar{\boldsymbol{N}} \cdot \bar{\boldsymbol{u}} = {}_{if}\boldsymbol{B} \cdot \bar{\boldsymbol{u}} \tag{5}$$

As shown in Fig. 4, three material axes are associated with the principal local axes of the element. Once ${}_{if}\boldsymbol{\varepsilon}_l$ are known, the local traction ${}_{if}\boldsymbol{\sigma}_l$ can be computed as:

$${}_{if}\boldsymbol{\sigma}_l = {}_{if}\boldsymbol{D}_l \cdot {}_{if}\boldsymbol{\varepsilon}_l \tag{6}$$

in which ${}_{if}\boldsymbol{D}_l$ is the constitutive matrix of the interface element in the local axes system.

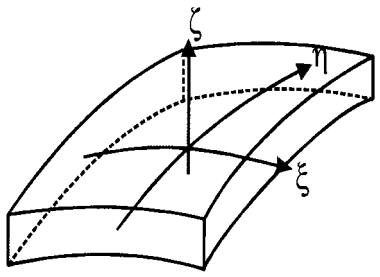

Fig. 4 Local interface element material axes (Scarpas 1992)

Eq. (6) can be expressed also in analytical form as:

$$\begin{Bmatrix} {}_{if}\sigma_{\xi} \\ {}_{if}\sigma_{\eta} \\ {}_{if}\sigma_{\zeta} \end{Bmatrix} = \begin{bmatrix} D_{\xi\xi} & D_{\xi\eta} & D_{\xi\zeta} \\ D_{\eta\xi} & D_{\eta\eta} & D_{\eta\zeta} \\ D_{\zeta\xi} & D_{\zeta\eta} & D_{\zeta\zeta} \end{bmatrix} \cdot \begin{Bmatrix} \Delta u_l \\ \Delta v_l \\ \Delta w_l \end{Bmatrix} \tag{7}$$

A lobatto scheme is used for numerical integration of the element equations.

2.2 Fluid component

The global pore fluid pressures of two originally coinciding points *j* and *k*, one on each side of the element, Fig. 3, can be expressed in terms of the nodal pore fluid pressures as:

$$\begin{Bmatrix} p^k \\ p^j \end{Bmatrix} = \begin{bmatrix} 0 & 0 & 0 & \cdots & 0 & N_1 & N_2 & N_3 & \cdots & N_8 \\ N_1 & N_2 & N_3 & \cdots & N_8 & 0 & 0 & 0 & \cdots & 0 \end{bmatrix} \begin{Bmatrix} p_1 \\ p_2 \\ p_3 \\ \cdots \\ \cdots \\ p_{14} \\ p_{15} \\ p_{16} \end{Bmatrix} \tag{8a}$$

or

$$\boldsymbol{p} = \bar{\boldsymbol{N}} \cdot \bar{\boldsymbol{p}} \tag{8b}$$

Similar as Eq. (3), the jump of pore fluid pressure through the interface thickness can be defined as:

$$\Delta p_{\zeta} = [1 \ -1] \begin{Bmatrix} p^k \\ p^j \end{Bmatrix} \tag{9a}$$

in which ζ indicates the normal axes of the element. Substituting Eq. (8) into Eq. (9a):

$$\begin{aligned} \Delta p_{\zeta} &= [1 \ -1] \begin{bmatrix} 0 & 0 & 0 & \cdots & 0 & N_1 & N_2 & N_3 & \cdots & N_8 \\ N_1 & N_2 & N_3 & \cdots & N_8 & 0 & 0 & 0 & \cdots & 0 \end{bmatrix} \cdot \bar{\boldsymbol{p}} \\ &= \begin{bmatrix} -N_1 & -N_2 & \cdots & -N_8 & N_1 & N_2 & \cdots & N_8 \end{bmatrix} \cdot \bar{\boldsymbol{p}} \end{aligned} \tag{9b}$$

or

$$\Delta p_{\zeta} = \bar{\bar{\boldsymbol{N}}} \cdot \bar{\boldsymbol{p}} \tag{9c}$$

Because of the negligible thickness of the interface element, it is postulated that:

$$\frac{\partial p}{\partial \zeta}=\Delta p_{\zeta} \tag{10}$$

In this investigation, it is postulated that fluid can only flow in the normal direction of the interface. Therefore, by utilization of coordinate transformation, the relation between the gradient of pore fluid pressure in $\nabla \boldsymbol{p}$ in the global coordinate system and the gradient of pore fluid pressure in the local interface coordinate system is:

$$\nabla \boldsymbol{p}=\boldsymbol{T}^{T} \cdot \left\{ \begin{array}{ccc} 0 & 0 & \dfrac{\partial p}{\partial \zeta} \end{array} \right\}^{T}=T^{T} \cdot \{0 \;\; 0 \;\; \Delta p_{\zeta}\}^{T} \tag{11}$$

in which $\nabla=\{\partial/\partial x \;\; \partial/\partial y \;\; \partial/\partial z\}^{T}$. Substituting Eq. (9c) and Eq. (10) into Eq. (11), $\nabla \boldsymbol{p}$ can be written in terms of nodal pore pressure vector as:

$$\nabla \boldsymbol{p}=\boldsymbol{W} \cdot \bar{\boldsymbol{p}} \tag{12}$$

in which matrix $\boldsymbol{W}$ is the multiplication of $\boldsymbol{T}^{T}$ and $\overline{\overline{\boldsymbol{N}}}$.

The pore pressure field within the element can be defined in terms of average values of the nodal pore pressure on the two sides of the element as:

$$p=\overline{\boldsymbol{N}} \cdot \boldsymbol{S} \cdot \bar{\boldsymbol{p}} \tag{13}$$

where S = [1/2 1/2].

In the global axes system, according to the Darcy's law, the relation between fluid velocity $\boldsymbol{q}$ and pressure change $\nabla \boldsymbol{p}$ can be written as:

$$\boldsymbol{q}=\frac{\kappa}{\mu} \cdot \nabla \boldsymbol{p} \tag{14}$$

in which κ is the absolute permeability matrix of the element in the global system and μ is the dynamic viscosity of fluid. Similarly, in the interface element local system:

$$\boldsymbol{q}_{l}=\frac{\kappa_{l}}{\mu} \cdot \nabla_{l} \boldsymbol{p} \tag{15}$$

in which $\nabla_{l}=\{\partial/\partial \xi \;\; \partial/\partial \eta \;\; \partial/\partial \zeta\}^{T}$ and κ_{l} is the absolute permeability matrix of the element in the local system.

The relations of the fluid velocity and the pressure gradient between the global system and the interface local system can be expressed as:

$$\boldsymbol{q}=\boldsymbol{T}^{T} \cdot \boldsymbol{q}^{l} \tag{16}$$

and

$$\nabla \boldsymbol{p}=\boldsymbol{T}^{T} \cdot \nabla \boldsymbol{p}_{l} \tag{17}$$

Combining Eq. (14) to Eq. (17), it results :

$$\frac{\kappa}{\mu} \cdot \nabla \boldsymbol{p}=\boldsymbol{q}=\boldsymbol{T}^{T} \cdot \boldsymbol{q}_{l}=\boldsymbol{T}^{T} \cdot \frac{\kappa_{l}}{\mu} \cdot \nabla \boldsymbol{p}_{l}=\boldsymbol{T}^{T} \cdot \frac{\kappa_{l}}{\mu} \cdot \boldsymbol{T} \cdot \nabla \boldsymbol{p} \tag{18}$$

so that the transformation of permeability matrix from local axes system into the global axes system

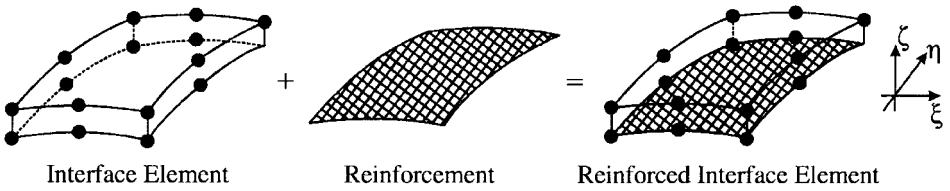

Fig. 5 Simulation of 3-D reinforced interface element

is obtained as:

$$\kappa = \boldsymbol{T}^T \cdot \kappa_l \cdot \boldsymbol{T} \tag{19}$$

2.3 Reinforcement component

In order to be capable of simulating the reinforcing function of some geotextile/geogrid systems utilized as *LS*, a reinforcement component was also implemented. The reinforcement component is assumed to be spanning along a layer perpendicular to the ζ axis of the element, Fig. 5. Within this layer, the direction of the reinforcement does not have to coincide with the direction of the principal axes of the element. More than one layers of reinforcement can be specified.

The isoparametric formulation of Eq. (1) is used to build the relation between the global coordinates and the coordinates of the element nodes. On the basis of this, in the element local axes system, the reinforcement strains are related to the element nodal displacements by means of the relation:

$$_{rf}\varepsilon_l = {}_{rf}\boldsymbol{B} \cdot \bar{\boldsymbol{u}} \tag{20}$$

in which ${}_{rf}\boldsymbol{B}$ is the standard global-nodal displacements to local-element-strains transformation matrix. In contrast to ${}_{rf}\boldsymbol{B}$, used in Eq. (5), ${}_{rf}\boldsymbol{B}$ contains spatial gradients of the shape functions.

Once the reinforcement strains ${}_{rf}\varepsilon_l$ are known, the stresses ${}_{rf}\sigma_l$ within the reinforcement can be computed as:

$$_{rf}\sigma_l = {}_{rf}\boldsymbol{D}_l \cdot {}_{rf}\varepsilon_l \tag{21}$$

in which ${}_{rf}\boldsymbol{D}_l$ is the constitutive matrix of the reinforcement component in the local element system.

The stresses and the strains of reinforcement in the global coordinate system can be computed from:

$$_{rf}\sigma = (\boldsymbol{T}')^T \cdot {}_{rf}\sigma_l \tag{22}$$

$$_{rf}\varepsilon = (\boldsymbol{T}'')^T \cdot {}_{rf}\varepsilon_l \tag{23}$$

in which $\boldsymbol{T}' = \boldsymbol{T}_1' \cdot \boldsymbol{T}_2'$ is the stress transformation matrix which consists of the transformation $\boldsymbol{T}_1'$ from local reinforcement axes to the local element coordinate system and $\boldsymbol{T}_2'$ from the local element coordinate system to the global element coordinate system. $\boldsymbol{T}''$ is the equivalent strain transformation matrix. A lobatto scheme is used for numerical integration of the element equations.

3. Basic governing formulations

The governing equations for simulating the interaction between the solid phase of the interface element and the fluid phase are developed on the basis of Biot's theory. The fluid flow through the element obeys Darcy's law. The principle of mass conservation holds for the fluid flow. Small strain theory will be applied for this investigation.

3.1 Equilibrium equation

By means of the principle of virtual work, for a set of virtual displacements $\delta\bar{\boldsymbol{u}}$, it can be shown that:

$$\begin{aligned}\delta\bar{\boldsymbol{u}}^T\cdot\boldsymbol{f}&=\int_{{}_{if}A}\ {}_{if}\delta\varepsilon_l^T\cdot{}_{if}\sigma_l\cdot d_{if}A+\int_{{}_{rf}V}\ {}_{rf}\delta\varepsilon_l^T\cdot{}_{rf}\sigma_l\cdot d_{rf}V\\&=\int_{{}_{if}A}\ {}_{if}\delta\varepsilon_l^T\cdot{}_{if}\sigma_l\cdot d_{if}A+{}_{rf}A\cdot\int_{{}_{rf}h}\ {}_{rf}\delta\varepsilon_l^T\cdot{}_{rf}\sigma_l\cdot d_{rf}h\end{aligned}\tag{24}$$

in which the *if* terms relate to the interface element and the *rf* relate to the reinforcing component; ${}_{if}A$ is the surface area of the interface; ${}_{rf}A$ is the surface area of the reinforcement component; ${}_{rf}h$ is reinforcement component length; $\boldsymbol{f}$ is the external forces applied at the element nodes.

According to Terzaghi's principle, the total stress σ_l may be split into the so-called effective stress σ_l' and excess pore pressure p as:

$$\sigma_l=\sigma_l'-\boldsymbol{I}\cdot p\tag{25}$$

and the entries of vector $\boldsymbol{I}$ corresponding to the normal stress components are 1. Otherwise they are 0. Tension is considered positive.

Substituting Eq. (25) into Eq. (24) and writing in incremental form:

$$\begin{aligned}\delta\bar{\boldsymbol{u}}^T\cdot d\boldsymbol{f}&=\int_{{}_{if}A\ if}\delta\varepsilon_l^T\cdot d({}_{if}\sigma_l'-\boldsymbol{I}\cdot p)\cdot d_{if}A+{}_{rf}A\cdot\int_{{}_{rf}h\ rf}\delta\varepsilon_l^T\cdot{}_{rf}d\sigma_l\cdot d_{rf}h\\&=\int_{{}_{if}A\ if}\delta\varepsilon_l^T\cdot{}_{if}d\sigma_l'\cdot d_{if}A-\int_{{}_{if}A\ if}\delta\varepsilon_l^T\cdot\boldsymbol{I}\cdot dp\cdot d_{if}A+{}_{rf}A\cdot\int_{{}_{rf}h\ rf}\delta\varepsilon_l^T\cdot{}_{rf}d\sigma_l\cdot d_{rf}h\end{aligned}\tag{26}$$

Substituting Eq. (5), Eq. (6), Eq. (20) and Eq. (21) into Eq. (26), it results in:

$$\begin{aligned}\delta\bar{\boldsymbol{u}}^T\cdot d\boldsymbol{f}&=\int_{{}_{if}A\ if}\delta\bar{\boldsymbol{u}}^T\cdot{}_{if}\boldsymbol{B}^T\cdot{}_{if}\boldsymbol{D}_l\cdot{}_{if}\boldsymbol{B}\cdot d\bar{\boldsymbol{u}}\cdot d)_{if}A-\int_{{}_{if}A\ if}\delta\bar{\boldsymbol{u}}^T\cdot{}_{if}\boldsymbol{B}^T\cdot\boldsymbol{I}\cdot dp\cdot d_{if}A\\&\quad+{}_{rf}A\cdot\int_{{}_{rf}h\ rf}\delta\bar{\boldsymbol{u}}^T\cdot{}_{rf}\boldsymbol{B}^T\cdot{}_{rf}\boldsymbol{D}_l\cdot{}_{rf}\boldsymbol{B}\cdot d\bar{\boldsymbol{u}}\cdot d_{rf}h\end{aligned}\tag{27}$$

Canceling $\delta\bar{\boldsymbol{u}}^T$ from both sides:

$$\begin{aligned}d\boldsymbol{f}&=\left\{\int_{{}_{if}A\ if}\boldsymbol{B}^T\cdot{}_{if}\boldsymbol{D}_l\cdot{}_{if}\boldsymbol{B}\cdot d_{if}A+{}_{rf}A\cdot\int_{{}_{rf}h\ rf}\boldsymbol{B}^T\cdot{}_{rf}\boldsymbol{D}_l\cdot{}_{rf}B\cdot d_{rf}h\right\}\cdot d\bar{\boldsymbol{u}}\\&\quad-\left\{\int_{{}_{if}A\ if}\boldsymbol{B}^T\cdot\boldsymbol{I}\cdot d_{if}A\right\}\cdot dp\end{aligned}\tag{28}$$

Substituting Eq. (13) into Eq. (28) and defining:

$$_{if}\boldsymbol{k}_e=\int_{_{if}A}\ {}_{if}\boldsymbol{B}^T\cdot{}_{if}\boldsymbol{D}_l\cdot{}_{if}\boldsymbol{B}\cdot d_{if}A \tag{29a}$$

$$_{if}\boldsymbol{k}_e={}_{rf}A\cdot\int_{_{rf}h}\ {}_{rf}\boldsymbol{B}^T\cdot{}_{rf}\boldsymbol{D}_l\cdot{}_{rf}\boldsymbol{B}\cdot d_{rf}h \tag{29b}$$

and

$$\boldsymbol{J}=-\int_{_{if}A}\ {}_{if}\boldsymbol{B}^T\cdot\boldsymbol{I}\cdot\bar{\boldsymbol{N}}\cdot\boldsymbol{S}\cdot d_{if}A \tag{29c}$$

Then Eq. (28) can be expressed as:

$$\boldsymbol{k}\cdot d\bar{\boldsymbol{u}}+J\cdot d\bar{\boldsymbol{p}}-d\boldsymbol{f}=0 \tag{30}$$

Dividing by time increment *dt*, the equilibrium equation that governs the response of the reinforced interface element is obtained:

$$\boldsymbol{k}\cdot\frac{d\bar{\boldsymbol{u}}}{dt}+\boldsymbol{J}\cdot\frac{d\bar{\boldsymbol{p}}}{dt}-\frac{d\boldsymbol{f}}{dt}=0 \tag{31}$$

in which $\boldsymbol{k}={}_{if}\boldsymbol{k}_e+{}_{rf}\boldsymbol{k}_e$ is the stiffness matrix of the element.

3.2 Continuity equation

Considering the geometric characteristics of the interface element, it is postulated that no storage of fluid takes place within the element. Then, according to the mass conservation principle, the flow entering the element should be equal to the flow leaving the element. Hence, the continuity equation of fluid flow through the interface element can be defined as:

$$A=\nabla^T\cdot(\rho\boldsymbol{q})=0 \tag{32}$$

in which $\boldsymbol{q}$ is the fluid velocity and ρ is the fluid density. On combining with Darcy's law, it results:

$$\bar{X}=\nabla^T\left(-\frac{\kappa}{\mu}\nabla(\boldsymbol{p}+\rho\ gh)\right)=0 \tag{33}$$

in which g is the gravity acceleration and h is the head above some arbitrary datum.

Flow through the element can be defined as:

$$\bar{Y}=-\boldsymbol{n}^T\frac{\kappa}{\mu}\nabla(\boldsymbol{p}+\rho\ gh)-\hat{q}=0 \tag{34}$$

in which $\boldsymbol{n}$ is the unit normal in the local ζ direction of the interface, $\hat{q}$ is the outflow rate per unit area of the boundary surface (Lewis *et al.* 1987).

Eq. (33) and Eq. (34) can be specified at all points within and on the boundary of the element domain by utilization of the weighted residual method (Zienkiewicz and Morgan 1983). Explicitly the Eq. (35) condition is imposed:

$$\int_{_{if}A}\ W^T\cdot\bar{X}\cdot d_{if}A+\int_{_{if}\Gamma}\ \tilde{W}^T\cdot\bar{Y}\cdot d_{if}\Gamma=0 \tag{35}$$

in which ${}_{if}\Gamma$ is the boundary of the element, W and $\tilde{W}$ are the weighting functions which, in general, can be chosen independently.

Substituting Eq. (33) and Eq. (34) into Eq. (35), it results:

$$\int_{if A} (\nabla W)^T \cdot \left(\frac{\kappa}{\mu}\nabla(\boldsymbol{p}+\rho g h)\right) \cdot d_{if} A + \int_{if\Gamma} \tilde{W}^T \cdot \boldsymbol{n}^T \frac{\kappa}{\mu}\nabla(\boldsymbol{p}+\rho g h) \cdot d_{if} + \int_{if\Gamma} \tilde{W}^T \cdot \hat{q} \cdot d_{if}\Gamma = 0 \quad (36)$$

In Eq. (36), the first integral may be written in weak form by using the well-known Green's theorem (Zienkiewicz 1977):

$$\int_\Omega \phi \frac{\partial \psi}{\partial x} d\Omega = -\int_\Omega \frac{\partial \phi}{\partial x} \psi d\Omega + \int_\Gamma (\phi\psi) n_x d\Gamma \quad (37)$$

where ϕ and ψ are suitable differentiable function, n_x, is the direction cosines of the outward normal to the boundary Γ. Applying this to the integrals in Eq. (36), we get:

$$\begin{aligned} &-\int_{if A} (\nabla W)^T \cdot \left(\frac{\kappa}{\mu}\nabla(\boldsymbol{p}+\rho g h)\right) \cdot d_{if} A + \int_{if\Gamma} W^T \cdot \boldsymbol{n}^T \frac{\kappa}{\mu}\nabla(\boldsymbol{p}+\rho g h) \cdot d_{if}\Gamma \\ &+\int_{if\Gamma} \tilde{W}^T \cdot \boldsymbol{n}^T \frac{\kappa}{\mu}\nabla(\boldsymbol{p}+\rho g h) \cdot d_{if}\Gamma + \int_{if\Gamma} \tilde{W}^T \cdot \hat{\boldsymbol{q}} \cdot d_{if}\Gamma = 0 \end{aligned} \quad (38)$$

By choosing the weight functions as:

$$\tilde{W} = -W|_{if\Gamma} \quad (39)$$

the terms involving the weighted integral of the gradient of pressure on the interface element boundary disappear and Eq. (38) reduces to:

$$\int_{if A} (\nabla W)^T \cdot \left(\frac{\kappa}{\mu}\nabla(\boldsymbol{p}+\rho g h)\right) \cdot d_{if} A + \int_{if\Gamma} W^T \cdot \hat{q} \cdot d_{if}\Gamma = 0 \quad (40)$$

By applying the Galerkin's approximation, the weight function W is replaced by the shape function $\bar{\boldsymbol{N}}\boldsymbol{S}$ defined in Eq. (13). The continuity condition at all points within and on the boundary of the element can be described by:

$$\int_{if A} (\nabla \bar{\boldsymbol{N}}\boldsymbol{S})^T \cdot \frac{\kappa}{\mu}\nabla \boldsymbol{p} \cdot d_{if} A + \int_{if\Gamma} (\bar{\boldsymbol{N}}\boldsymbol{S})^T \cdot \hat{q} \cdot d_{if}\Gamma + \int_{if A} (\nabla \bar{\boldsymbol{N}}\boldsymbol{S})^T \cdot \frac{\kappa}{\mu}\nabla \rho g h \cdot d_{if} A = 0 \quad (41)$$

Substituting $\nabla \boldsymbol{p}$ from Eq. (12) into Eq. (41) and considering the permeability transformation of Eq. (19):

$$\int_{if A} (\nabla \bar{\boldsymbol{N}}\boldsymbol{S})^T \cdot \boldsymbol{T}^T \cdot \frac{\kappa_l}{\mu} \cdot \boldsymbol{T} \cdot \boldsymbol{W} \cdot \bar{\boldsymbol{p}} \cdot d_{if} A + \int_{if\Gamma} (\bar{\boldsymbol{N}}\boldsymbol{S})^T \cdot \hat{q} \cdot d_{if}\Gamma + \int_{if A} (\nabla \bar{\boldsymbol{N}}\boldsymbol{S})^T \cdot \frac{\kappa}{\mu}\nabla \rho g h \cdot d_{if} A = 0 \quad (42)$$

For brevity, Eq. (41) can be written in matrix form:

$$\boldsymbol{H} \cdot \bar{\boldsymbol{p}} + \boldsymbol{Q} = 0 \quad (43)$$

where

$$\boldsymbol{H} = \int_{if A} (\nabla \bar{\boldsymbol{N}}\boldsymbol{S})^T \cdot \boldsymbol{T}^T \cdot \boldsymbol{T} \cdot \frac{\kappa}{\mu} \cdot \boldsymbol{T}^T \cdot \bar{\bar{\boldsymbol{N}}} \cdot d_{if} A \quad (44a)$$

$$\boldsymbol{Q} = \int_{if\Gamma} (\bar{\boldsymbol{N}}\boldsymbol{S})^T \cdot \hat{q} \cdot d_{if}\Gamma + \int_{if A} (\nabla \bar{\boldsymbol{N}}\boldsymbol{S})^T \cdot \frac{\kappa}{\mu}\nabla \rho g h \cdot d_{if} A \quad (44b)$$

Eq. (31) and Eq. (43) constitute the governing equations for simulation of the interaction between the solid and fluid components of the element. In the following section, a time stepping algorithms will be presented for their simultaneous solution.

3.3 Time discretization and incremental equation

The complete solution of Eq. (31) and Eq. (43) can be obtained by means of appropriate time stepping algorithms. Assume that the solution for displacement and pore pressure is known at two time intervals t_1 and $t_1+\Delta t$. The time domain is divided into a number of steps and integration is carried out for each step to obtain the displacement $\bar{\boldsymbol{u}}$ and $\bar{\boldsymbol{p}}$.

There are many available schemes for the numerical time discretization (Zienkiewicz 1985). Here the discretization in time domain is carried out by the generalized trapezoidal method in which it is assumed:

$$X=(1-\theta)\cdot X^{t_1}+\theta\cdot X^{t_1+\Delta t} \tag{45}$$

where X^{t_1}, $X^{t_1+\Delta t}$, X are state vectors (displacements $\bar{\boldsymbol{u}}$ and pore pressures $\bar{\boldsymbol{p}}$) at time instants t_1, $t_1+\Delta t$ and t. $\theta=(t-t_1)/\Delta t$ is a time discretization parameter, usually in the range [0–1].

In order to ensure unconditional numerical stability conditions for soil water interaction, $\theta \geq 0.5$ is recommended (Zienkiewicz 1985).

For small time step length Δt, the time derivative of Eq. (45) can be written as:

$$\begin{aligned}\frac{dX}{dt}&=\frac{d(1-\theta)}{dt}X^{t_1}+\frac{d\theta}{dt}X^{t_1+\Delta t}\\&=\frac{1}{-\Delta t}X^{t_1}+\frac{1}{\Delta t}X^{t_1+\Delta t}\end{aligned} \tag{46}$$

By means of Eq. (46), the displacements $\bar{\boldsymbol{u}}$ and pore pressure $\bar{\boldsymbol{p}}$ in Eq. (31) can be discretized in time to obtain:

$$\boldsymbol{k}\cdot\left[\frac{1}{-\Delta t}\bar{\boldsymbol{u}}^{t_1}+\frac{1}{\Delta t}\bar{\boldsymbol{u}}^{t_1+\Delta t}\right]+\boldsymbol{J}\cdot\left[\frac{1}{-\Delta t}\bar{\boldsymbol{p}}^{t_1}+\frac{1}{\Delta t}\bar{\boldsymbol{p}}^{t_1+\Delta t}\right]-\frac{\Delta \boldsymbol{f}}{\Delta t}=0 \tag{47}$$

Multiplying Eq. (47) by Δt and rearranging it results:

$$\boldsymbol{k}\cdot\bar{\boldsymbol{u}}^{t_1+\Delta t}+\boldsymbol{J}\cdot\bar{\boldsymbol{p}}^{t_1+\Delta t}=\boldsymbol{k}\cdot\bar{\boldsymbol{u}}^{t_1}+\boldsymbol{J}\cdot\bar{\boldsymbol{p}}^{t_1}+\Delta\boldsymbol{f} \tag{48}$$

In a similar way, $\bar{\boldsymbol{p}}$ in Eq. (43) can be discretized via Eq. (45) to obtain:

$$\boldsymbol{H}\cdot\theta\cdot\bar{\boldsymbol{p}}^{t_1+\Delta t}=\boldsymbol{H}\cdot\theta\cdot\bar{\boldsymbol{p}}^{t_1}-\boldsymbol{H}\cdot\bar{\boldsymbol{p}}^{t_1}-\boldsymbol{Q} \tag{49}$$

In incremental form, Eq. (48) and Eq. (49) can be expressed as:

$$\boldsymbol{k}\cdot\Delta\bar{\boldsymbol{u}}+\boldsymbol{J}\cdot\Delta\bar{\boldsymbol{p}}=\Delta\boldsymbol{f} \tag{50}$$

$$\boldsymbol{H}\cdot\theta\cdot\Delta\bar{\boldsymbol{p}}=-\boldsymbol{H}\cdot\bar{\boldsymbol{p}}^{t_1}-\boldsymbol{Q} \tag{51}$$

in which, $\Delta\bar{\boldsymbol{u}}=\bar{\boldsymbol{u}}^{t_1+\Delta t}-\bar{\boldsymbol{u}}^{t_1}$, $\Delta\bar{\boldsymbol{p}}=\bar{\boldsymbol{p}}^{t_1+\Delta t}-\bar{\boldsymbol{p}}^{t_1}$.

In matrix format, Eq. (50) and Eq. (51) can be written as:

$$\begin{bmatrix} \boldsymbol{k} & \boldsymbol{J} \\ 0 & \theta \cdot \boldsymbol{H} \end{bmatrix} \begin{bmatrix} \Delta \bar{\boldsymbol{u}} \\ \Delta \bar{\boldsymbol{p}} \end{bmatrix} = \begin{bmatrix} \Delta f \\ -\boldsymbol{H}\bar{\boldsymbol{p}}^{t_1} - \boldsymbol{Q} \end{bmatrix} \tag{52}$$

In Eq. (52), the coupling between the fluid and the solid components becomes apparent. It forms the basis of the finite element implementation of the reinforced interface element in the finite elements system INSAP-PM (Liu undated) which was developed at TU-Delft.

4. Finite element simulation of lining system

In order to gain some insight about the mechanism and phenomena involved in the transfer of forces between a LS and the surrounding materials, two different LS were considered. One consists of a bituminous layer and another consists of a layer of asphalt concrete. By employing the two-phase interface element, the influence of consolidation on the stress distribution along the LS was evaluated. Parametric FE element analyses were performed for various combinations of material characteristics. The case of the LS being reinforced with a geogrid was also considered.

4.1 Finite element modeling and material characteristics

The same mesh was utilized for both the reservoir and the landfill case. Because of symmetry, only half of the structure was simulated. The geometry of the finite element mesh and the specified boundary conditions are shown in Fig. 6. Free drainage was assumed at the boundaries of the mesh.

For the reservoir, hydrostatic water pressure of 0.15 MPa at the bottom of the mesh was applied for a 10 years period. For the landfill structure, a linearly increasing, over a period of two years, pressure of 0.75 MPa due to dumping of waste materials was applied. The pressure was assumed constant after the two years period. In both simulations, the self-weight of the surrounding materials was also taken into account.

To investigate the long term behavior due to consolidation, low permeability clay was chosen as the underlying soil material, Table 1. The mechanical properties of LS materials were experimentally

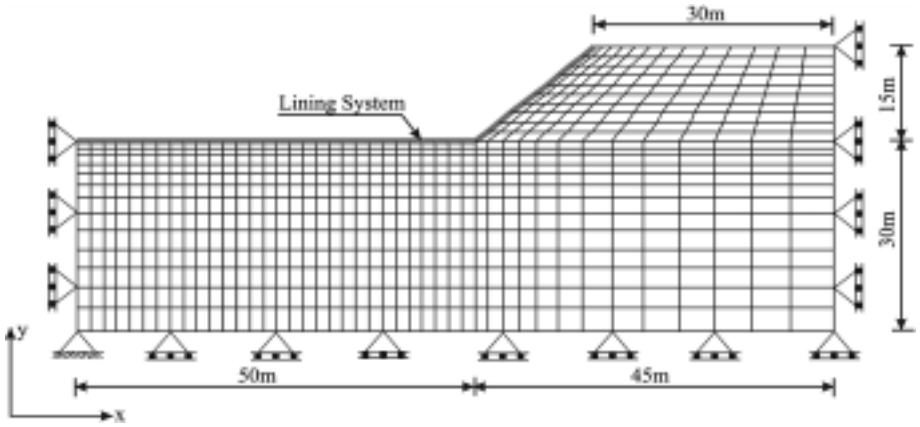

Fig. 6 Schematic of reservoir/landfill geometry characteristics

Table 1 Material parameters

Table 1	Soil	Bitumen	Asphalt concrete	Reinforcement
Young's modulus (MPa)	10	1	100	various
Layer thickness (mm)		5	100	1
Permeability (mm/sec)	1.0e-06			
Density (kg/m^3)	2000			

determined. An impervious LS was simulated.

4.2 In time system response

4.2.1 Reservoir structure

In the case of the reservoir, the gradual, with time, redistribution of excess pore water pressure in the underlying soil material can be seen from Fig. 7. At early stages of loading, higher values of excess pore water pressure occur in the soil underneath the bituminous LS, Fig. 7(a). However, due to the drainage of water continuously from the horizontal boundaries of the structure, excess pore water pressure decrease in time, Fig. 7(b).

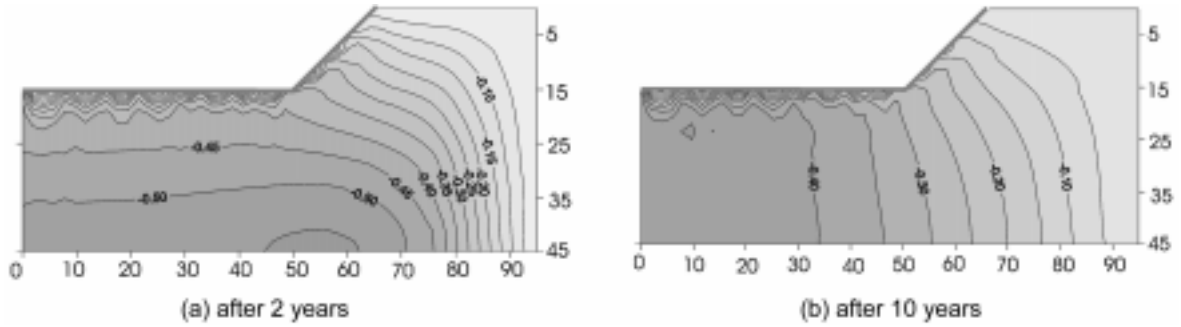

Fig. 7 Contours of excess pore water pressure at different times around the reservoir

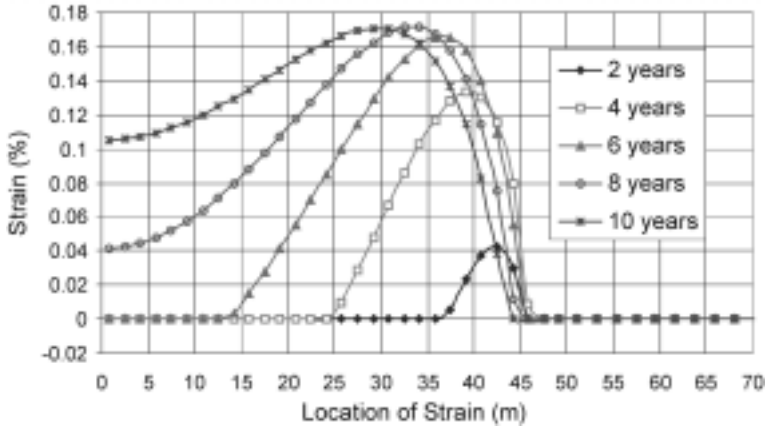

Fig. 8 Strain distribution along bituminous layer at different times in reservoir

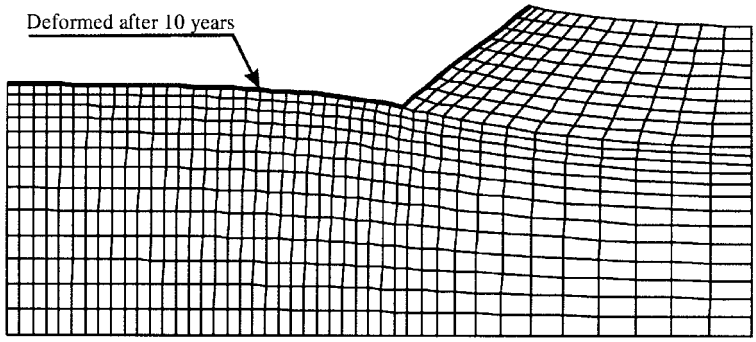

Fig. 9 Deformed mesh of the reservoir structure with bituminous LS (10 times enlarged)

The reduction of excess pore water pressure results to increasing deformations at the base of the reservoir. This causes gradual strain redistribution in the bituminous layer, Fig. 8. Because of soil consolidation, the area of highest deformation in the bituminous layer gradually shifts toward the center of the reservoir. At the same time, the magnitude of tensile strains increases.

The deformed mesh of the reservoir structure, after ten years of soil consolidation, is shown in Fig. 9. Due to the high self-weight of the surrounding materials and the relatively low hydrostatic water pressure at the bottom of the reservoir, the maximum vertical displacement at the bottom of the sloping edge of the reservoir is about 0.3 m after 10 years.

4.2.2 Landfill structure

In the landfill case, because the applied load is much higher than that in the reservoir, significant increase in the magnitude of tensile strains in the bituminous layer is observed, Fig. 10. During the design process it is imperative that allowance is made for such a large elongation of the lining layer during the lifetime of the structure. It can be also observed that the critical deformation area is located at the center of the landfill.

For the case of the landfill with an asphalt concrete LS, significant increase of strains within the asphalt is observed with time, Fig. 11. Comparison with conventional experimental results on

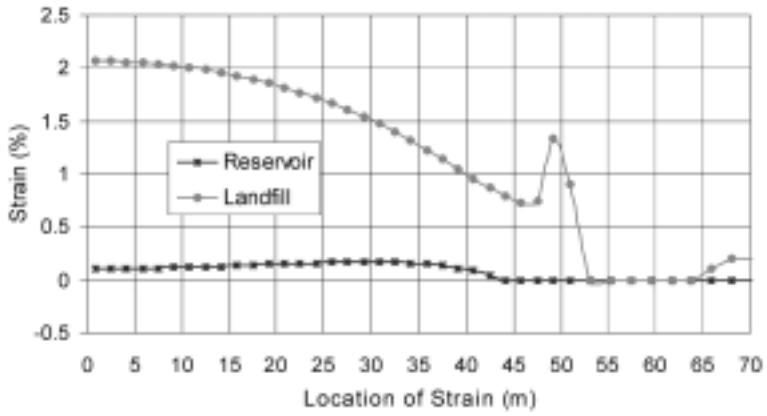

Fig. 10 Comparison of strain distribution along the bituminous layer at 10 years

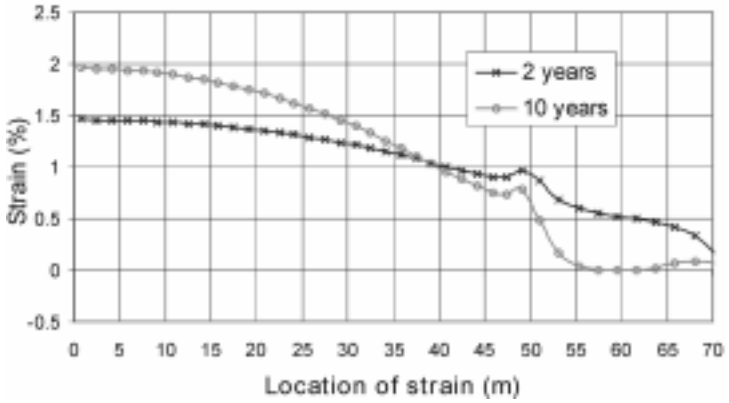

Fig. 11 Strain distribution along the asphalt concrete layer in landfill at different times

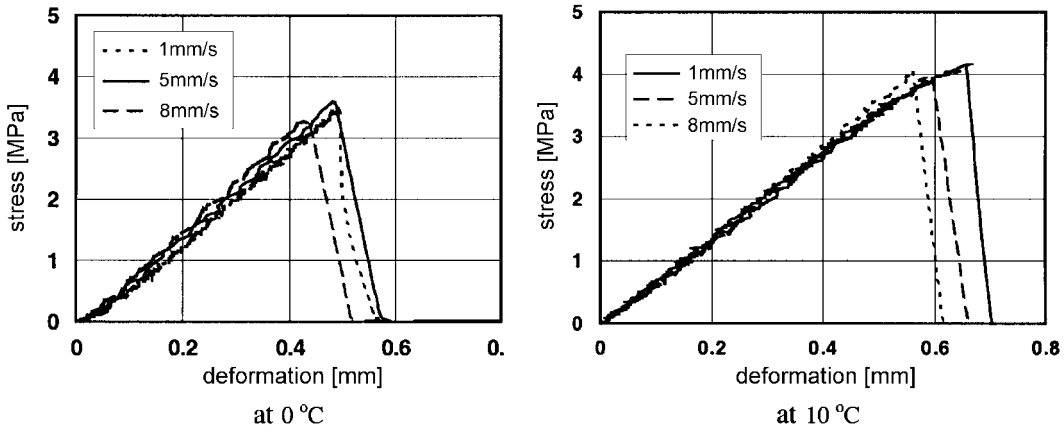

Fig. 12 Asphalt tensile test results at different temperatures

asphalt concrete, Fig. 12, indicates that the required tensile strain exceeds the experimentally obtained ultimate strain of the material. Hence, unless appropriate measures are taken, leakage may

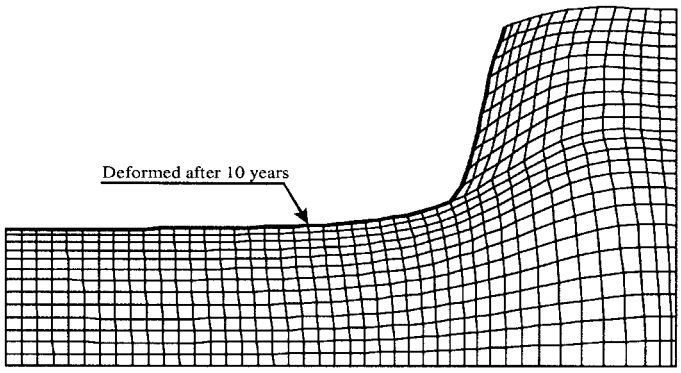

Fig. 13 Deformed mesh of the landfill structure with asphalt concrete LS (20 times enlarged)

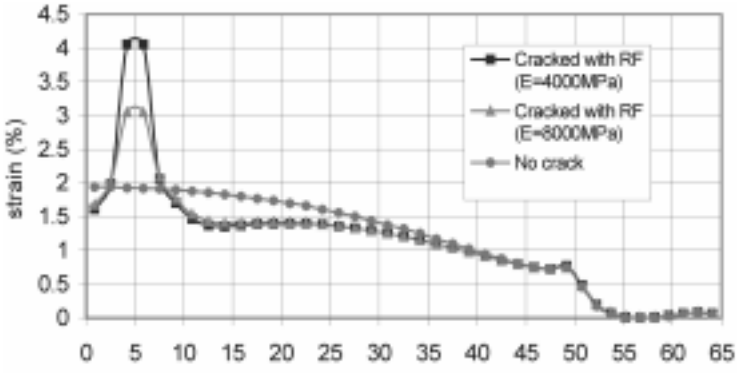

Fig. 14 Influence of reinforcement on the strain distribution along the asphalt concrete layer in landfill (10 years)

occur.

Fig. 13 shows the deformation of the landfill structure with asphalt concrete LS after ten years of soil consolidation. It can be observed that during soil consolidation, the settlement at the base of the landfill is quite uniform. The vertical displacement at the center is about 0.5 m after two years and 0.68 m after ten years.

4.2.3 Reinforcement

In order to investigate the capability of reinforcement embedded within the LS, to improve the transfer of forces after a crack has developed in the asphalt material, the landfill mesh was modified. A layer of reinforcement was introduced in the middle of the asphalt concrete lining layer. A crack in the asphalt concrete layer was simulated by artificially reducing the stiffness of the appropriate element at a distance of 5 m from the center of the LS.

For the non-cracked asphalt concrete lining layer, the strain distribution after 10 years is shown in Fig. 14. For comparison, the strain distributions, after cracking, corresponding to two different reinforcement stiffness values are also shown in Fig. 14. It can be concluded that stiffer reinforcement reduces the local deformations of the LS at the vicinity of the crack.

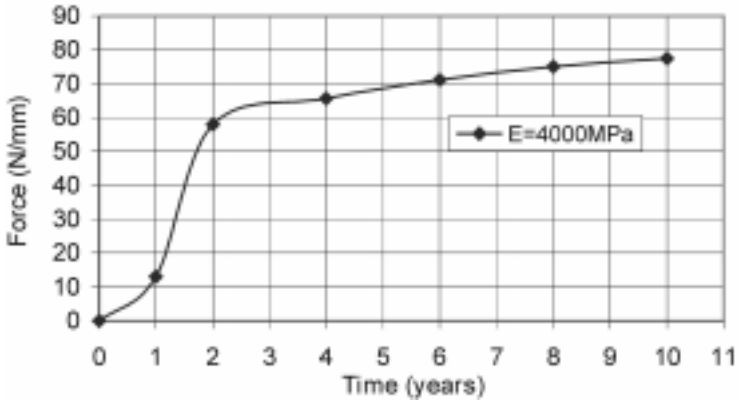

Fig. 15 In time force development in reinforcement for landfill

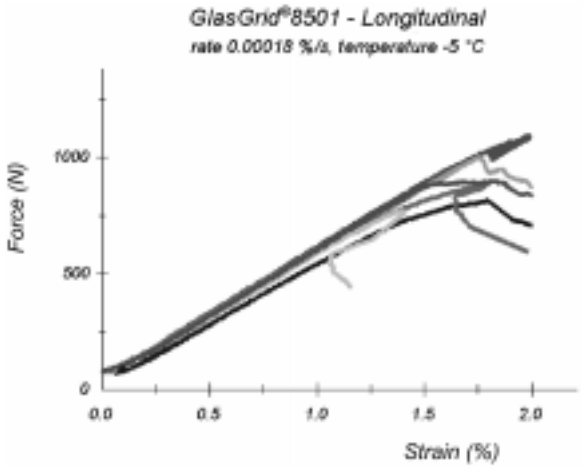

Fig. 16. Measured force versus strain of reinforcement strands

For the case of landfill with reinforced asphalt concrete LS, the in time development of the force in the reinforcement is presented in Fig. 15. At early stages of loading, due to the higher rate of soil consolidation, the rate of force increase in the reinforcement is high. After two years, because the rate of soil consolidation is reduced, the rate of force increase diminishes.

Fig. 16 shows the tensile strength of GlasGrid®8501 reinforcement tested at a temperature of −5ºC and a strain rate of 0.00018%/s for six individual strands. Assuming an average number of 78.6 bars/m. Tensile strength of this type of reinforcement is computed from Fig. 16 as 4032 N/mm with a coefficient of variation of 4.4% (de Bondt 1999). Comparison with Fig. 15 indicates that this type of reinforcement would have been adequate to resist the forces generated due to consolidation of the underlying material of the landfill.

5. Conclusions

An isoparametric two-phase interface element has been developed capable of simulating the interaction between the mechanical behavior and the flow characteristics of LS. Coupling between the solid and the fluid phase is achieved by means of Biot's theory. Examples of the utilization of the two-phase interface element for the study of the in time performance of the LS in reservoir/ landfill structures have been presented.

References

de Bondt, A.H. (1999), "Special applications of sealoflex® bitumen", *Proc. of Sealoflex® World Conf.*, 1999, Tokyo, Japan, April.

Gens, A., Carol, I., and Alonso, E.E. (1988), "An interface element formulation for the analysiss of soil-reinforcement interaction", *Comput. and Geotech.*, **7**, 133-151.

Liu, X., Scarpas, A., and Blaauwendraad, J. (1999), "An interface element for porous media simulation", *Proc. of 1st Int. Conf. on Advances in Struct. Eng. and Mech.*, Seoul, Korea, August.

Liu, X. (undated), "Numerical simulation of porous media response under static and dynamic loads", Faculty of

Civil Engineering, TU-Delft, The Netherlands (PhD thesis, under preparation).
Lewis, R.W., and Schrefler, B.A. (1987), *The Finite Element Method in the Deformation and Consolidation of Porous Media*, John Wiley, New York.
Mehlhorn, G., Kollegger, J., Keuser, M., and Kolmar, W. (1985), "Non-linear contact problems: A finite element approach implemented in ADINA", *Comput. and Struct.*, **21**(1/2), 69-80.
Plesha, M.E., Ballariui, R., and Parulekar, A. (1989), "Constitutive model and finite element procedure for dilatant contact problems", *Int. J. Eng. Mech.*, ASCE, **115**(12), 2649-2668.
Schellekens, J.C.J., (1990), "Interface element in finite element analyses", Rep. No. 25-2-90-5-17, Delft University of Technology, 82.
Scarpas, A. (1992), "CAPA-3D finite elements system", *User's Manual, Parts I, II and III*, Faculty of Civil Engineering, TU-Delft.
Scarpas, A., Ehrola, E., and Judycki, J. (1994), "Simulation of load transfer across joints in reinforced concrete pavements", *Proc. of 3rd Int. Workshop on the Design and Evaluation of Concrete Pavements*, CROW Record 14, 249-258.
Ziekiewicz, O.C. (1977), *The Finite Element Method*, 3rd ed., McGraw-Hill, London.
Ziekiewicz, O.C., and Morgan, K. (1983), *Finite Element and Approximations*, John Wiley, Chicester.
Ziekiewicz, O.C., and Taylor, R.L. (1985), "Coupled problems- A simple time stepping procedure", *Comm. Appl. Numer. Meth.*, **1**, 233-239.